SUBJECT: **Flux Conversion and RSRF correction for the SPIRE FTS**

PREPARED BY: **Trevor Fulton, Edward Polehampton, Jean-Paul Baluteau, Bruce Swinyard**

DOCUMENT No: **SPIRE-BSS-REP-003243**

ISSUE: **1.0** **Date:** **29 January 2010**

APPROVED BY: **Date:**

Distribution

Name

SPIRE ICC

Change Record

ISSUE	DATE	Changes
Draft 0.1	18 November 2009	First version
Draft 0.2	28 January 2010	Replaced Fortuna OD122 observations with Vesta OD209 observations for point source calibration. Added point-source comparisons between measured and modelled spectra for Uranus and Neptune
Issue 1.0	29 January 2010	Added extended calibration section, and issue for ICC review

TABLE OF CONTENTS

Glossary

BDA	Bolometer Detector Array
CBB	Cold Blackbody
CR	Calibration Resolution
DCU	Detector Control Unit
FT	Fourier Transform
HR	High Resolution
LHS	Left Hand Side
LPF	Low-pass filter
LR	Low Resolution
MPD	Mechanical Path Difference
MR	Medium Resolution
NHKT	Nominal Housekeeping Timeline Product
OD	Operational Day
OPD	Optical Path Difference
RHS	Right Hand Side
RSRF	Relative Spectral Response Function
SDI	Spectrometer Detector Interferogram Product
SDS	Spectrometer Detector Spectrum Product
SDT	Spectrometer Detector Timeline Product
SMECT	Spectrometer MEChanism Timeline Product
SLW	Spectrometer Long Wavelength array
SMEC	Spectrometer MEChanism
SNR	Signal to noise ratio
SPIRE	Spectral and Photometric Imaging REceiver
SSW	Spectrometer Short Wavelength array
TBD	To Be Determined
TBW	To Be Written
ZPD	Zero Path Difference

1. INTRODUCTION

The purpose of this document is to describe the procedure used to derive the flux conversion and RSRF correction curves for the SPIRE Spectrometer detectors. A distinction is made between the conversion curves applicable to point sources and those applicable to extended sources.

1.1 Scope

1.2 Documents

1.2.1 Applicable Documents

Number	Document Name	Document Number	Issue
AD01	SPIRE Spectrometer Pipeline Description	SPIRE-BSS-DOC-002966	1.2
AD02	Delivery of Calibration Data From External Sites to RAL	http://www.herschel.be/twiki/bin/view/Spire/SpireIntDoc030700	

1.2.2 Reference Documents

RD01	PFM4 CBB/SCAL Transmission Analysis	SPIRE-BSS-REP-002769	0.2
RD02	Asteroids as calibration standards in the thermal infrared for space observatories	Müller, T. G.; Lagerros, J. S. V., Astronomy and Astrophysics, v.381, p.324-339 (2002)	
RD03	SPIRE Photometer Flux Density Calibration	SPIRE-UCF-DOC-3168	5
RD04	The Near Millimeter Brightness Temperature Spectra of Uranus and Neptune	Griffin, M.J. & Orton, G.S., Icarus, 105, 537, 1993.	
RD05	SPIRE Sensitivity Models	SPIRE-QMW-NOT-000642	

2. BACKGROUND

One of the final steps of the SPIRE spectrometer data processing pipeline [**AD01**] involves Flux Conversion and RSRF correction. The purpose of this step is to translate each of the measured spectra processed to that point ($V_{IN-i}(\sigma)$), from linearized voltage quantities with units of V*/(cm^{-1}) to optical power quantities with units of either Watts/m^2/(cm^{-1}) or Janskys]. This conversion is applied on a wavenumber-by-wavenumber basis as in equation 1 below

$$I_{OUT-i}(\sigma) = V_{IN-i}(\sigma) \times f_i(\sigma) \tag{1}$$

where $I_{OUT-i}(\sigma)$ is the flux calibrated output, $f_i(\sigma)$ is a table of Flux Conversion/RSRF correction factors (one per wavenumber bin), and i represents the detector index.

Implicit in equation 1 is the assumption that the correction factor includes the following:

1. a factor for the RSRF at a particular wavenumber for a given detector, $RSRF_i(\sigma)$,
2. a factor for the étendue at a particular wavenumber for a given detector, $A\Omega_i(\sigma)$,
3. and a flux conversion factor that converts the measured values to those with units of optical power, $F_i(\sigma)$.

As such, equation 1 can be restated to explicitly show these different factors, as in equation 2.

$$I_{OUT-i}(\sigma) = V_{IN-i}(\sigma) \times RSRF_i(\sigma) \times A\Omega_i(\sigma) \times F_i(\sigma) \tag{2}$$

In principle, one can also use the equation above to derive the conversion factors $f_i(\sigma)$ for each spectrometer detector from a measured spectrum, $V_{IN-i}(\sigma)$, and a known expected output flux $I_{OUT-i}(\sigma)$. Then the Flux Conversion, RSRF correction, and étendue terms for a particular detector can be derived as in equation 3:

$$f_i(\sigma) = RSRF_i(\sigma) \times A\Omega_i(\sigma) \times F_i(\sigma) = \frac{I_{OUT-i}(\sigma)}{V_{IN-i}(\sigma)} \tag{3}$$

3. ANALYSIS

The analysis section is divided into two main parts: one that describes the steps taken to derive the reference interferogram calibration product used to correct the on-source or target observations; the second section describes the steps taken to produce the measured spectra, from which the eventual flux conversion calibration information is to be derived using equation 3 in §2.

3.1 Common Processing Steps

The data processing steps that are common to both the reference observations and the on-source or target observations are shown in block form in Figure 3.1 below. These data processing steps follow closely those of the SPIRE Spectrometer data processing pipelines [**AD01**] up to the stage of interferogram creation.

1. **Extract Timelines.** This step simply extracts the three timelines relevant to a SPIRE spectrometer observation (SDT, SMECT, NHKT) for further processing.
2. **Non-linearity Correction.** The intent of this processing step is to eliminate from the detector timelines any non-linear responsivity effects.
3. **Temperature Drift Correction.** The intent of this processing step is to eliminate from the detector timelines effects due to low frequency thermal drifts.

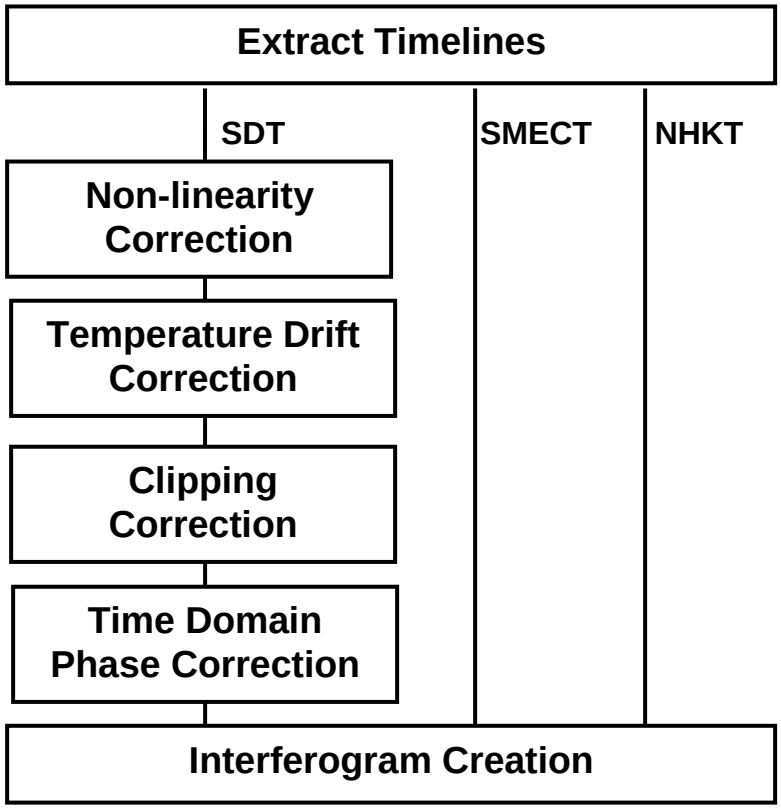

Figure 3.1: Block diagram of the common processing steps applied to both on-source and reference observation.

4. **Clipping Correction.** The intent of this processing step is to correct samples that have been truncated by the limits of the analogue-to-digital readout.
5. **Time Domain Phase Correction.** The intent of this processing step is to eliminate from the detector timelines the delay that is incurred by the read-out electronics and the bolometer thermal response. This processing step is described in detail in [**AD01**].
6. **Interferogram Creation.** The processed signals in the detector timelines are now merged with the mirror positions in the mechanism timeline to create a set of interferograms.

3.1.1 Creating Reference Interferograms

It is at this point where, the processing of the reference observations and of the Source or target observations diverges. The reference observations are each processed to create a single reference interferogram per detector – one interferogram per scan direction. The processing steps applied to the reference observations are described below and are shown in Figure 3.2.

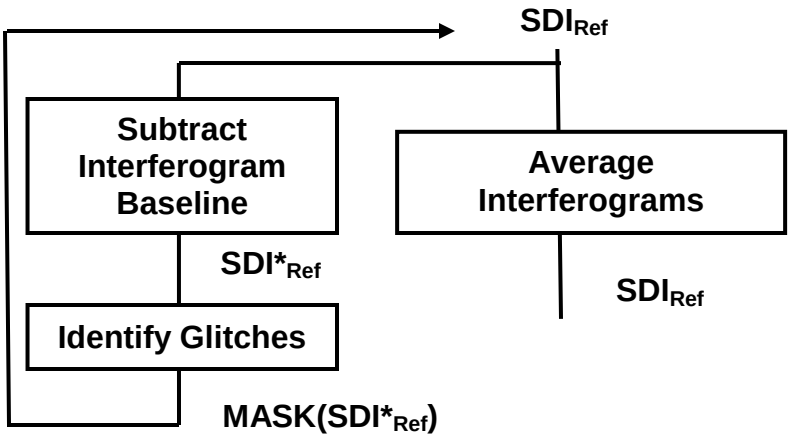

Figure 3.2: Block diagram of the steps applied to create the reference interferograms.

1. **Subtract Interferogram Baseline.** This step removes from the recorded interferograms an opd-dependant baseline. The baseline in characterized on an interferogram-by-interferogram basis as a 4th order polynomial. The correction is performed by subtraction of the fitted polynomial.
2. **Glitch Identification.** The glitch identification portion of the second level deglitching step is a then applied to the reference interferograms. The mask information after this step is then fed back to the interferogram product as it was just after interferogram creation.
3. **Average Interferograms.** The interferograms in the product as it was just after interferogram creation are then averaged on an opd-by-opd basis for each channel in the interferogram product. The SMEC scan direction and the presence of glitches are taken into account in this step – those samples identified as glitches are not considered in the averaging.

3.1.2 Processing Difference Interferograms

The block diagram of the processing steps for the difference interferograms is shown in Figure 3.3. The processing steps are described in more detail below.

1. **Subtract Reference Interferogram.** This processing step subtracts on a detector-by-detector basis, the average reference interferograms from each of the on-source interferograms created by the common processing steps. This processing step takes the SMEC scan direction into account.
2. **2nd-Level Deglitching.** This processing step identifies and removes any glitches remaining in the on-source interferograms.
3. **Transform and Phase Correct.** This processing step transforms the each difference interferogram to the spectral domain. There, the in-band portion of the phase is evaluated and a 2nd order weighted polynomial is fit to the phase. The fitted phase is then removed from the spectrum by multiplication. Finally, the corrected spectra are transformed back to the interferogram domain.

4. **Pad and Transform.** This processing step transforms the phase-corrected interferograms created in the previous step back to spectra. Prior to transformation, each interferogram is padded with zeros to ensure that the sampling interval of the resultant spectra is made to be uniform for all of the observations under consideration.
5. **Average.** The spectra for each detector are averaged on a wavenumber-by-wavenumber basis.

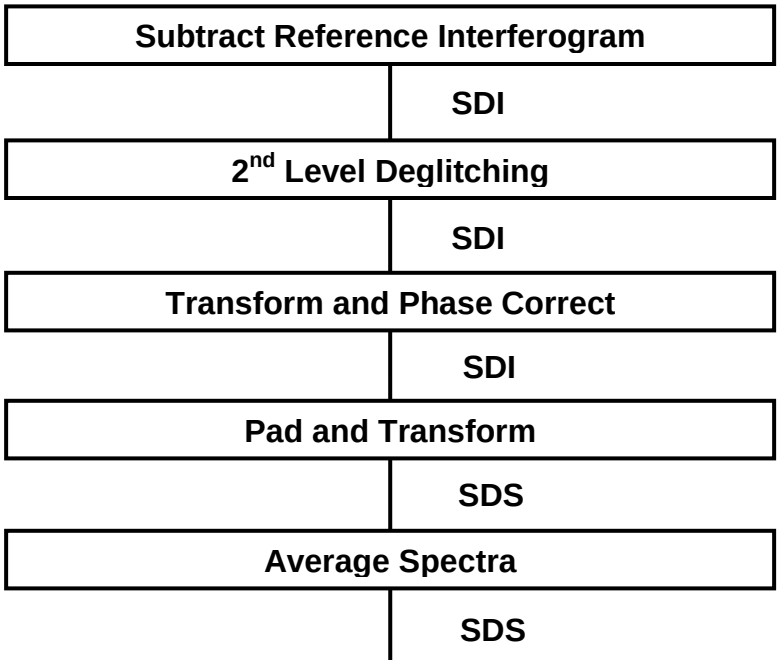

Figure 3.3: Block diagram of the final processing steps applied to the on-source observation data.

4. RESULTS

4.1 Point Source Flux Calibration

4.1.1 On Source and Reference Observations

Some of the criteria for determining whether a source is suitable for usage as a calibration source include the following:

1. its flux should be known,
2. its spectrum should be featureless.

One such suitable candidate is the asteroid 4 Vesta, which was observed extensively on OD 209 (see Table 1 below).

Observation ID	Astronomical Target	Target Detector (Co-Al)	Repetitions	Spectral Resolution
0x50002979	4 Vesta	SSWD4 (SLWC3)	50	CR
0x5000297A	4 Vesta	SSWC5 (SLWB3)	40	CR
0x5000297B	4 Vesta	SSWF3 (SLWC2)	40	CR
0x5000297C	4 Vesta	SSWC2 (SLWD3)	40	CR

Table 1: Observations used to derive the point source Flux Conversion/étendue/RSRF calibration information

As can be seen from the observations listed in Table 1, 4 Vesta was observed on four sets of target detectors on OD209. As 4 Vesta is a point source for the SPIRE spectrometer, its radiation will only be incident upon the target detectors; all other SPIRE detectors will simultaneously observe the Dark Astronomical Sky. As such, the reference interferograms (see §3.1.1) for each target detector pair can therefore be derived by combining the interferograms for those detectors from the other three observations of 4 Vesta. That is, the reference interferograms for SLWC3 and SSWD4 (OBSID=0x50002979) can be derived from the interferograms for those detectors from OBSIDs={0x5000297B, 0x5000297C, 0x5000297D}; likewise for the other target detector pairs.

The spectra, $V_{IN\text{-}i}(\sigma)$, from eq. 3, for each target detector are shown in Figure 4.1 and Figure 4.2.

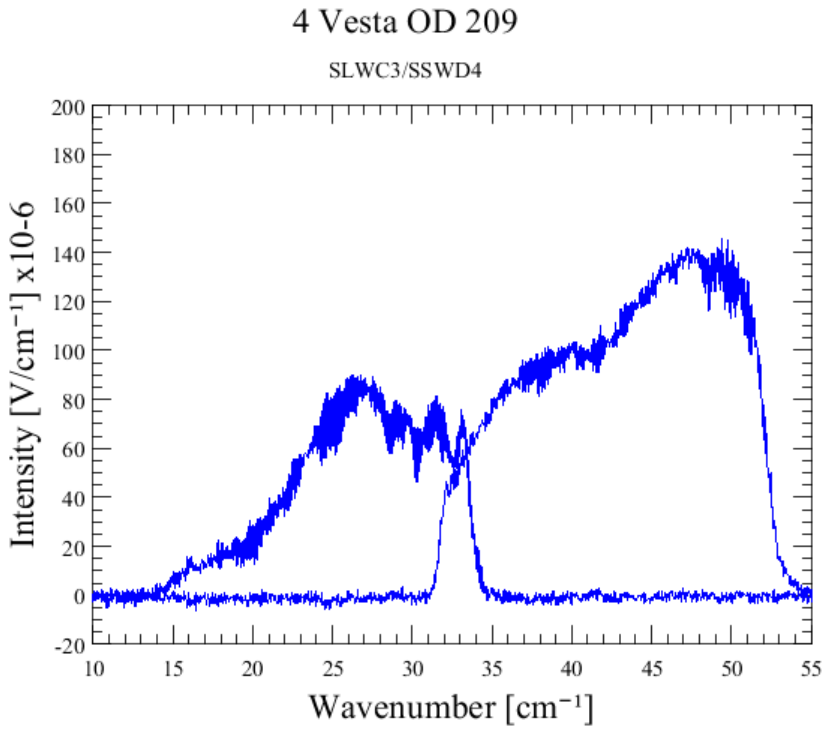

Figure 4.1: Average spectra derived from the OD209 observation of 4 Vesta (Central Detectors, OBSID=0x50002979).

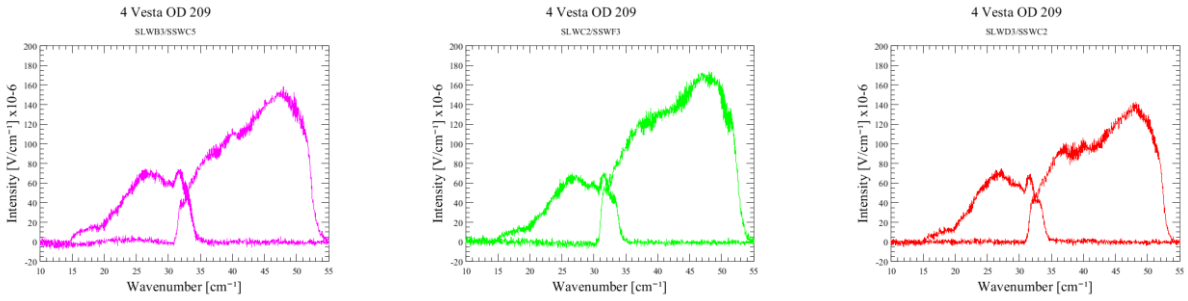

Figure 4.2: Average spectra derived from the OD209 observation of 4 Vesta, off-axis detectors. Left: SLWB3/SSWC5 (OBSID=0x5000297A), Middle: SLWC2/SSWF3 (OBSID=0x5000297B), Right: SLWD3/SSWC2 (OBSID=0x5000297C).

4.1.2 Model Flux

The expected flux densities of 4 Vesta for the observations from OD209, $I_{OUT\text{-}i}(\sigma)$, from eq. 3, are given by the thermophysical models of Thomas Müller [RD02] and are shown in Figure 4.3.

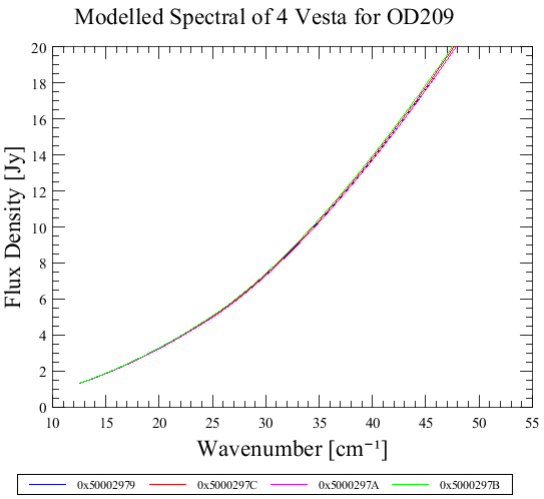

Figure 4.3: Modelled Flux Density of 4 Vesta for the calibration observations on OD 209. [RD02]

4.1.3 Derived Flux Calibration Product

The curves shown in Figure 4.1, Figure 4.2, and Figure 4.3 represent $V_{IN\text{-}i}(\sigma)$ and $I_{OUT\text{-}i}(\sigma)$, from eq. 3 for each of the four target detector pairs observed on OD209. The point-source Flux Conversion, RSRF correction, and étendue correction curves, $f_{\text{-}i}(\sigma)$, for these detectors can therefore be derived as the ratio of $I_{OUT\text{-}i}(\sigma)$ to $V_{IN\text{-}i}(\sigma)$. These curves are shown in Figure 4.4.

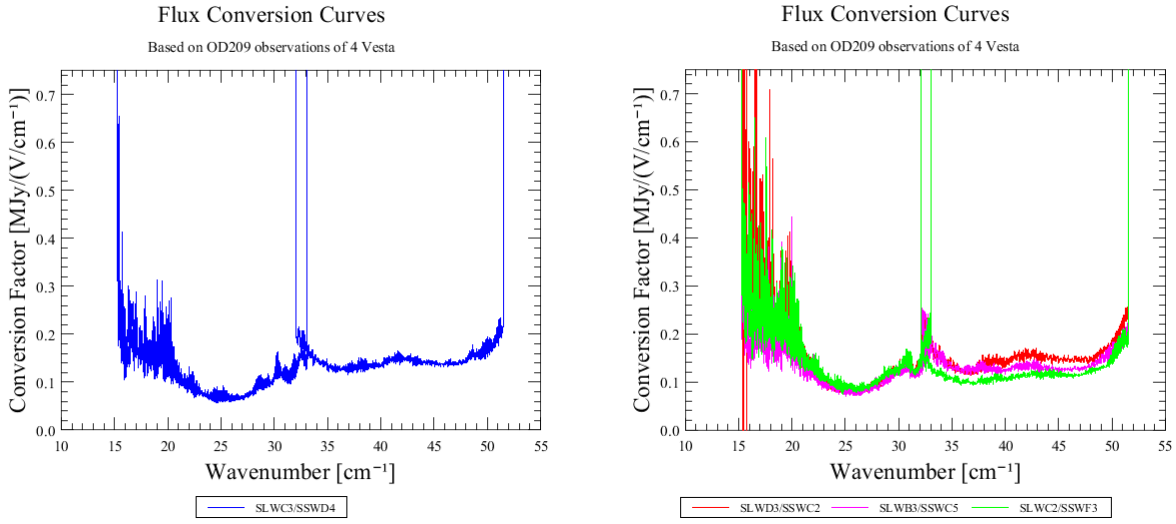

Figure 4.4: Point-source Flux Conversion and RSRF Correction curves derived from the OD209 observations of 4 Vesta. Left: Central detectors. Right: Off-axis detectors.

4.1.4 Flux Accuracy

In addition to the 4 Vesta calibration source, the planets Uranus and Neptune were also observed on OD209 (see Table 2. These observations, together with the Modified Griffin and Orton models {RD03, RD04] can be used to assess the accuracy of the point-source flux densities achieved using the calibration curves derived from 4 Vesta.

Observation ID	Astronomical Target	Target Detector (Co-Al)	Repetitions	Spectral Resolution
0x50002968	Uranus	SSWD4 (SLWC3)	4	HR
0x5000296B	Neptune	SSWC2 (SLWD3)	4	HR
0x5000296C	Neptune	SSWC5 (SLWB3)	4	HR
0x5000296D	Neptune	SSWF3 (SLWC2)	4	HR
0x5000296F	Neptune	SSWD4 (SLWC3)	4	CR

Table 2: Observations used to evaluate the accuracy of the flux calibration curves derived from observations of 4 Vesta

Each of the observations listed in Table 2 were processed to the level of average spectra, $V_{IN\text{-}i}(\sigma)$ (see §3.1.2). The spectral intensities were then converted to flux densities $I_{OUT\text{-}i}(\sigma)$ as in eq. 1, using the calibration curves $f_i(\sigma)$ shown in Figure 4.4. The resultant flux densities compared with the expected flux densities for Uranus and Neptune (SLWC3 and SSWD4) are shown in Figure 4.5, while the ratio of the model flux densities to the measured flux densities are shown in Figure 4.6.

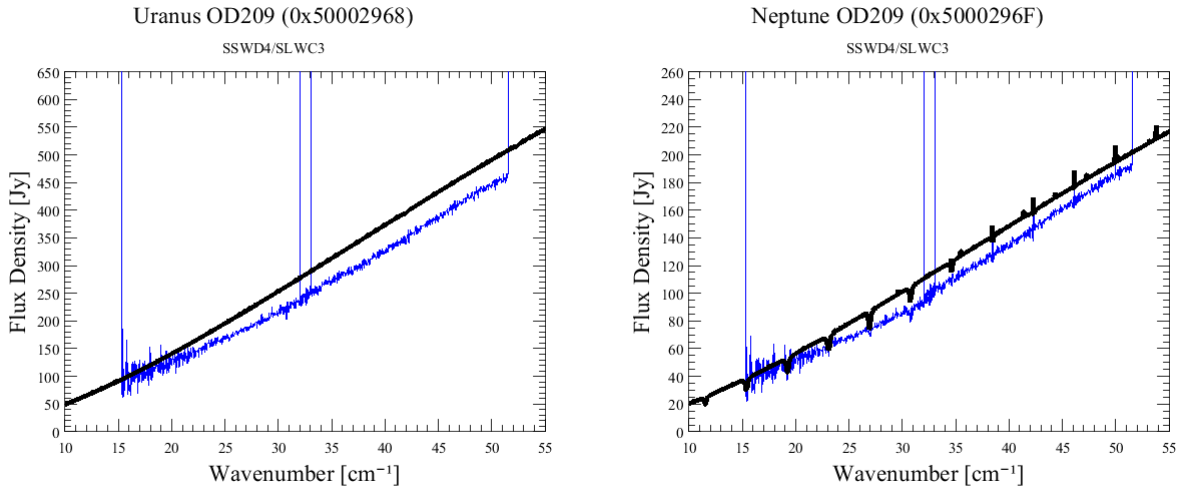

Figure 4.5: Planetary Spectra derived using the 4 Vesta flux conversion curves. Left: Uranus and model [RD03, RD04]. Right: Neptune and model [RD03, RD04].

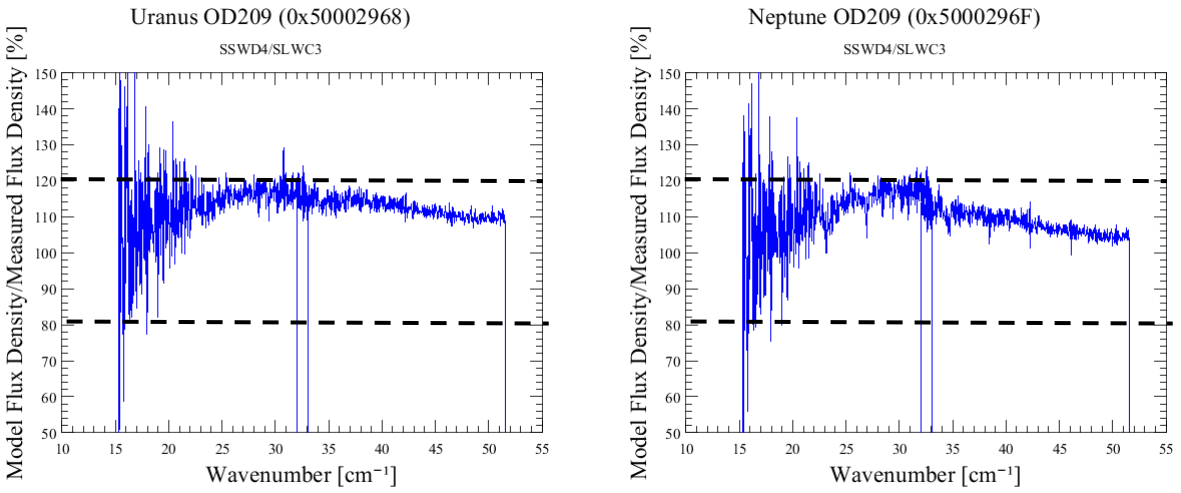

Figure 4.6: Ratio of the model to the measured, 4 Vesta-calibrated planetary spectra. Left: Uranus [RD03, RD04]. Right: Neptune [RD03, RD04]. The dashed lines represent agreement within 20%.

As can be seen from the curves in Figure 4.6, the Vesta-calibrated planetary spectra agree with their modelled spectra to within 20% across the entire wavenumber range for the two central detectors. Also apparent from the curves in Figure 4.5 and Figure 4.6 is that the Vesta-calibrated spectra are systematically lower than the model predictions.

As a first attempt to correct for the systematic differences, the flux conversion calibration curves were multiplied by a factor of 1.2. The ratios of the planetary models and the newly calibrated measured spectra are shown in Figure 4.7 and Figure 4.8.

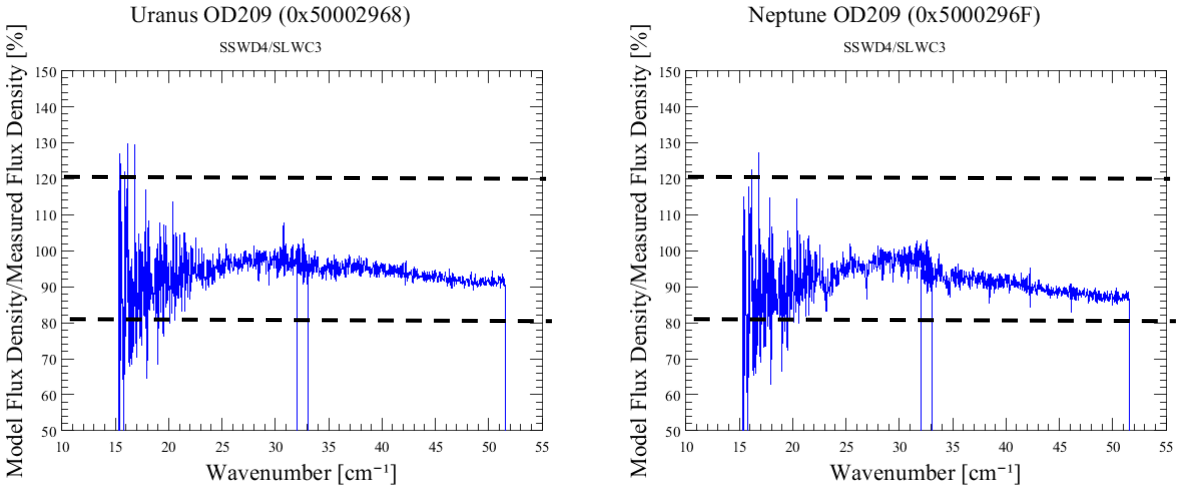

Figure 4.7: Ratio of the model to the measured, 4 Vesta-calibrated (x1.2) planetary spectra. Left: Uranus [RD03, RD04]. Right: Neptune [RD03, RD04]. The dashed lines represent agreement within 20%.

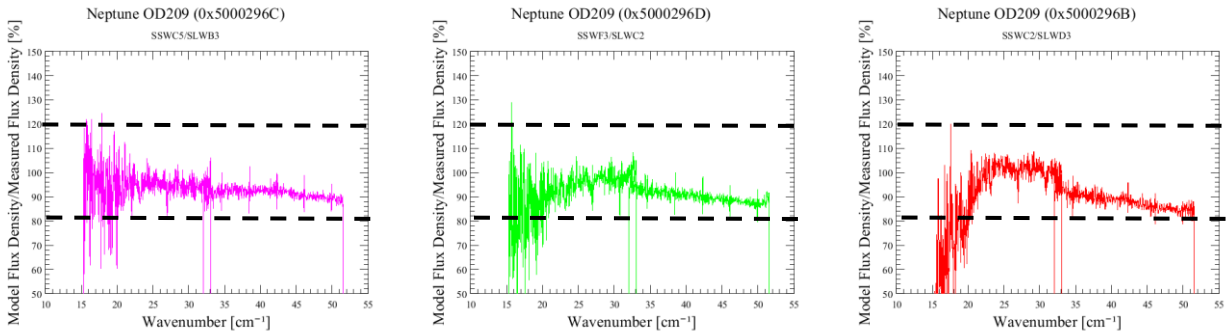

Figure 4.8: Ratio of the model to the measured, 4 Vesta-calibrated (x1.2) Neptune spectra, off-axis detectors. Left: SLWB3/SSWC5 [RD03, RD04]. Middle: SLWC2/SSWF3 [RD03, RD04]. Right: SLWD3/SSWC2 [RD03, RD04]. The dashed lines represent agreement within 20%.

4.1.5 Future Work

Future versions of this portion of this document will:

1) include a correction of thermal variations of SPIRE instrument to attempt reduce the noise at the long wavelengths;
2) compare of point and extended source curves;
3) include a measure of the uncertainty in the point-source flux conversion calibration curves.

4.2 Extended Source Flux Calibration

The emission from the telescope provides a good means to calculate a calibration for flat and uniformly extended sources. This can be achieved by using the temperatures of the instrument and telescope to derive a model of the observed flux from the dark sky.

4.2.1 Instrument and Telescope Model

A model of the telescope emission has been set up by splitting the input flux into components from different parts of the instrument.

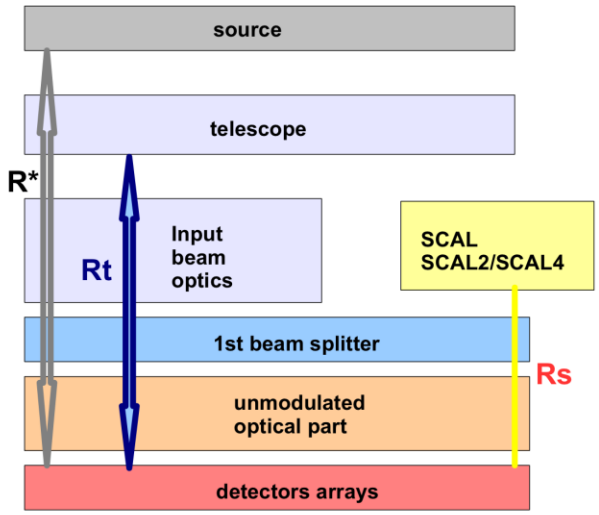

Figure 4.9: Schematic showing the different components included in the instrument and telescope model

In the following, the RSRF is combined with the throughput ($A\Omega$) to give the flux conversion factors R^*, R_t and R_s for the source, the telescope and the SCAL box respectively.

R^* is expected to change from a point source to a uniformly extended source and should depend critically on the source morphology.

So, with this basic view, we expect that any measurement is the sum of different components,

$$Measurement = R^* B_{source} + R_t B_{tel} + R_s (X_{input} B_{input} - B_{scals})$$

where,
B_{source} is the source brightness (SED),
B_{tel} the emission from the telescope (see below),
B_{input} the Plank function for the temperature of the optics in the input beam,
B_{scals} the combined emission from the SCAL port (see below),
X_{input} is an unknown function which combines the effective emissivity of the input beam optics and any departure from the assumed R_s

The emission from the telescope is determined using its emissivity (see RD05),

$$\varepsilon_{tel} = 0.0336\lambda^{-0.5} + 0.273\lambda^{-1}$$

where λ is wavelength in microns. The final emission from the telescope, assuming that there is no stray light, and taking account of emission from both the primary and secondary mirrors, and reflection from the secondary, is,

$$B_{tel} = (1-\varepsilon_{tel})\varepsilon_{tel} B(T_{M1},\sigma) + \varepsilon_{tel} B(T_{M2},\sigma)$$

where $B(T,\nu)$ is the Planck function, calculated using frequency so that the final units can be easily converted to Jy,

$$B(T,\nu) = \frac{2h\nu^3}{c^2}\frac{1}{e^{h\nu/kT}-1}$$

The combined emission from the SCAL port is given by,

$$B_{scals} = 0.02B(T_{SCAL2},\nu) + 0.04B(T_{SCAL4},\nu) + 0.94B(T_{SCAL},\nu)$$

The method to determine the different elements in the model relies on subtraction of data with slightly different values for the temperatures.

4.2.2 The SCAL Port, R_s

For SLW, the following pairs of observations were used:

Dark 1	OD	SCAL temp	Dark 2	OD	SCAL temp
0x50001AC5	130	15 K	0x50001AD6	131	OFF
0x5000265F	189	15 K	0x5000264E	189	OFF
0x50001ACB	130	25 K	0x50001AD6	131	OFF

For SSW, only observations after the bias change on OD189 were used:

Dark 1	OD	SCAL temp	Dark 2	OD	SCAL temp
0x5000265F	189	15 K	0x5000264E	189	OFF

The telescope temperatures were assumed to be the same for these observations.

Method:

- Reduce Dark 1 to interferograms using clipping, nonlinearity, temp drift & time domain phase corr., combining all building blocks
- Use the reference interferogram calibration file for Dark 2 (which has had the same processing applied. It contains two separate average interferograms – one for forward scans and one for reverse scans)
- Subtract Dark 2 from Dark 1 using the *telescopeScalSubtraction* task
- Process the difference interferograms to spectra (one forward, one reverse) using baseline subtraction, 2nd level deglitch, phase correction, FT and averageSpectra
- Calculate B_{scals} for each observation as above

- Calculate Rs from the difference spectrum for each scan direction,

$$R_s = \frac{(S_1 - S_2)}{(B_{scals-1} - B_{scals-2})}$$

R_s was calculated for each pair of observations, and for each scan direction. These were averaged together over all pairs of observations, but kept separate for the different scan directions.

The full table of telescope and instrument temperatures for the observation is shown in Sect 4.2.5.

The calculation makes some important assumptions, i.e. that R_s is the same for the three components (SCAL2, SCAL4 and SCAL). We know from the ground measurements that the RSRF from SCAL2 and SCAL4 exhibits some significant differences. However for SCAL we have no information about its RSRF compared to that of SCAL2 (it is in fact very difficult to get it now, in space). There certainly should be some significant differences as SCAL can be considered extended but SCAL2 is not.

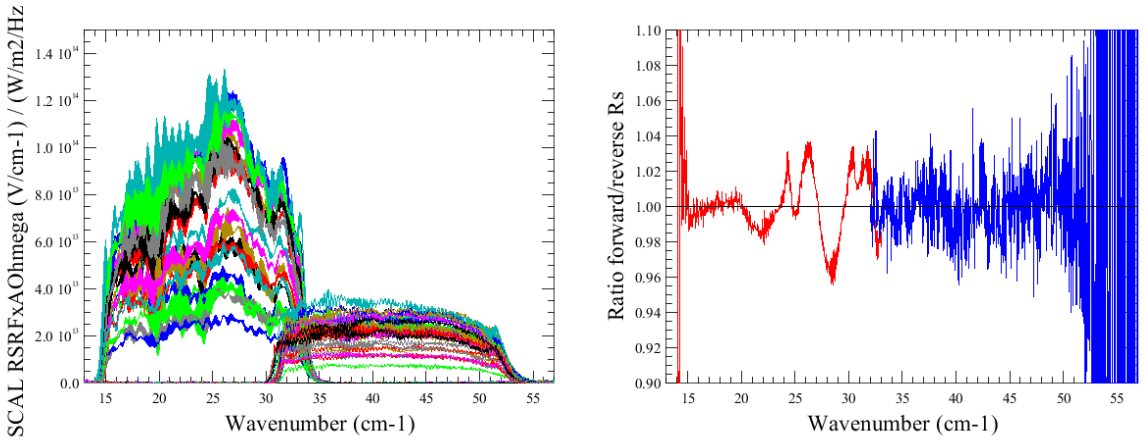

Figure 4.10: The final R_s function (SCAL RSRF×AΩ) for every detector in the array for reverse scans. The wide variation in amplitude is due to the different levels of vignetting towards the edge of the array. The units are V/cm^{-1} per W/m^2/Hz/sr. The right hand plot shows the ratio of R_s for forward and reverse scans for the central detectors.

4.2.3 The Contribution from the Instrument, X_{in}

For SLW, three pairs of observations were used in which there was a variation in the instrument temperatures.

Dark 1	OD	SCAL temp	Dark 2	OD	SCAL temp
0x50001995	123	OFF	0x50001AD6	131	OFF
0x50001AD6	131	OFF	0x5000264E	189	OFF
0x50001AC5	130	15 K	0x5000265F	189	15 K

For SSW, the instrument makes a much smaller contribution to the measured flux so there is very low signal to noise in any subtraction. Therefore, a constant value of 0.75 was used for SSW, extrapolated from the end of the SLW band. This will need to be revisited later in the mission when more data are available.

Method:

- Reduce Dark 1 to interferograms using clipping, nonlinearity, temp drift & time domain phase corr., combining all building blocks
- Use the reference interferogram calibration file for Dark 2 (which has had the same processing applied, It contains two separate average interferograms – one for forward scans and one for reverse scans)
- Subtract Dark 2 from Dark 1 using the *telescopeScalSubtraction* task
- Process the difference interferograms to spectra (one forward, one reverse) using baseline subtraction, 2nd level deglitch, phase correction, FT and averageSpectra
- Calculate B_{scals}, B_{tel} and B_{input} for each observation as above
- Calculate the instrument temperature as an average of the following sensor values: SCAL2TEMP, SCAL4TEMP, SCALTEMP
- Calculate X_{in} from the difference spectrum for each scan direction, taking a value for Rs as calculated in the previous section, and an estimate of R_t calculated assuming a constant value of X_{in}=0.75,

$$X_{in} = \frac{(S_1 - S_2) - R_t(B_{tel\_1} - B_{tel\_2}) + R_s(B_{scals\_1} - B_{scals\_2})}{R_s(B_{input-1} - B_{input-2})}$$

X_{in} was calculated for each pair of observations, and for each scan direction. These were averaged together over all pairs of observations, but kept separate for the different scan directions.

The full table of telescope and instrument temperatures for the observation is shown in Sect. 4.2.5.

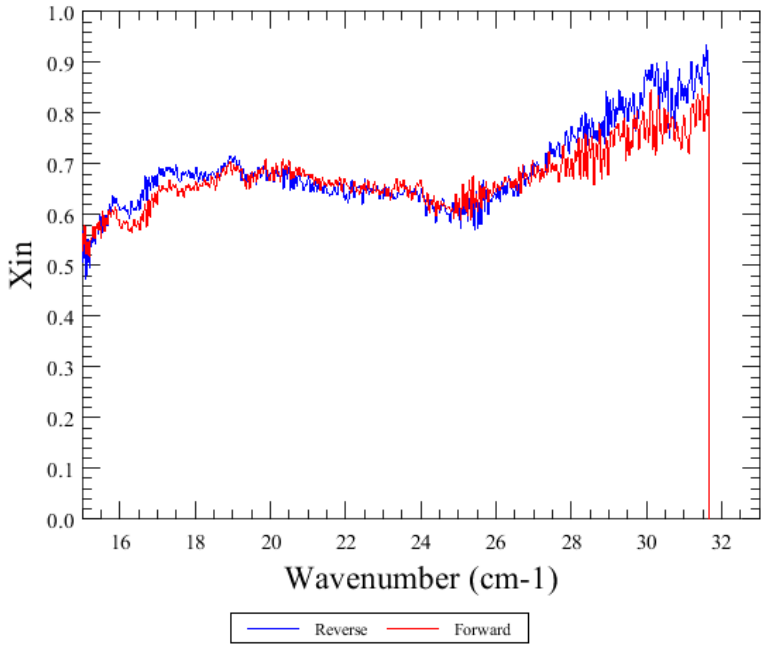

Figure 4.11: The X_{in} function for the centre detector of SLW (C3) for forward and reverse scans derived from 0x50001995 and 0x50001AD6.

4.2.4 The Telescope, R_t

For the final calculation of R_t, only a few observations are used because there are no measurements yet with sufficiently different telescope temperatures. This will improve as more measurements are made through the mission.

Three observations were used and the results averaged together:

Observation	OD	SCAL temp
0x50001995	123	OFF
0x50001AD6	131	OFF
0x5000264E	189	OFF

Method:

- Reduce observation to interferograms using clipping, nonlinearity, temp drift & time domain phase corr., combining all building blocks
- Process the interferograms to spectra (one forward, one reverse) using baseline subtraction, 2nd level deglitch, phase correction, FT and averageSpectra
- Calculate B_{scals}, B_{tel} and B_{input} for each observation as above
- Read in R_s and X_{in} as calculated above
- Calculate the instrument temperature as an average of the following sensor values: SCAL2TEMP, SCAL4TEMP, SCALTEMP
- Calculate R_t using,

$$R_t = \frac{S - R_s(X_{in}B_{input} - B_{scals})}{B_{tel}}$$

The final instrument temperatures for these observations are shown in Sect. 4.2.5.

The final flux calibration is applied as a multiplication, so is equal to $1/R_t$. Forward and reverse scans were kept separate up to this point, but the two were averaged to produce the final flux conversion calibration product.

The units of the final product should be W/m2/Hz/sr/(V/cm^{-1}), which can easily be changed to MJy/sr/(V/cm^{-1}) by multiplying by 10^{20}.

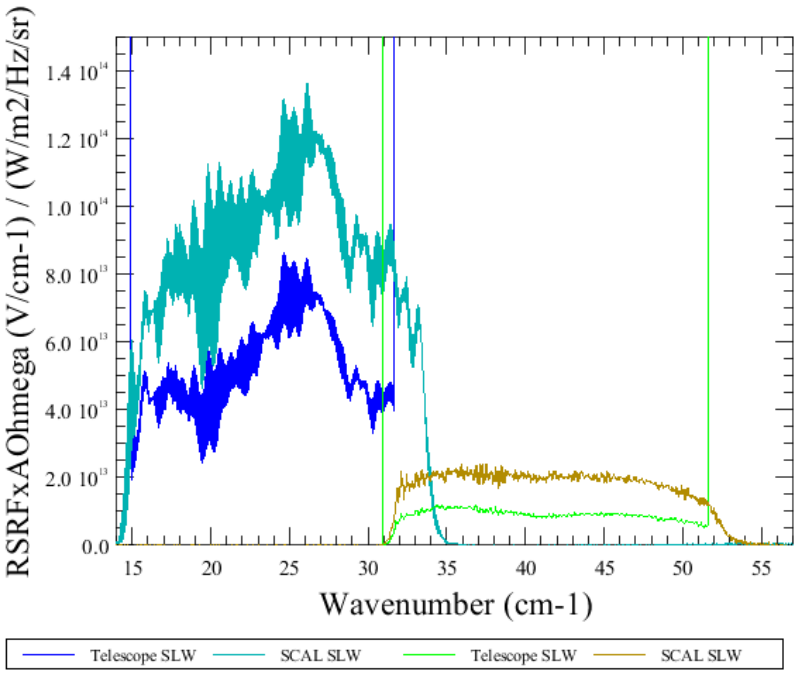

Figure 4.12: The telescope function, R_t, compared to the SCAL function, R_s for the central detectors (SSWD4 and SLWC3).

4.2.5 Temperatures in the Observations used

The full list of telescope and instrument temperatures for all of the observations used for the extended source calculations are:

Observation	SCAL2 temp	SCAL4 temp	SCAL temp	M1 temp	M2 temp
0x50001AC5	15.0008	5.2134	5.1180	86.7609	83.2381
0x50001AD6	5.2494	5.1544	5.0695	86.7978	83.2602
0x5000265F	15.0009	4.6297	4.5325	87.8429	84.1196
0x5000264E	4.6059	4.5243	4.4385	87.8149	84.1127
0x50001ACB	25.0017	5.2603	5.1419	86.7820	83.2460
0x50001995	4.7233	4.6384	4.5521	86.6265	83.1406

4.2.6 Future Work

Future versions of this portion of this document will:

1) include a check of the extended source calibration using Neptune;
2) include more pairs of dark sky observations as they are observed;